

Solution NMR study of the yeast cytochrome *c* peroxidase: cytochrome *c* interaction

Alexander N. Volkov · Nico A. J. van Nuland

Received: 12 April 2013 / Accepted: 13 May 2013 / Published online: 25 May 2013
© Springer Science+Business Media Dordrecht 2013

Abstract Here we present a solution NMR study of the complex between yeast cytochrome *c* (Cc) and cytochrome *c* peroxidase (CcP), a paradigm for understanding the biological electron transfer. Performed for the first time, the CcP-observed heteronuclear NMR experiments were used to probe the Cc binding in solution. Combining the Cc- and CcP-detected experiments, the binding interface on both proteins was mapped out, confirming that the X-ray structure of the complex is maintained in solution. Using NMR titrations and chemical shift perturbation analysis, we show that the interaction is independent of the CcP spin-state and is only weakly affected by the Cc redox state. Based on these findings, we argue that the complex of the ferrous Cc and the cyanide-bound CcP is a good mimic of the catalytically-active Cc–CcP compound I species. Finally, no chemical shift perturbations due to the Cc binding at the low-affinity CcP site were observed at low ionic strength. We discuss possible reasons for the absence of the effects and outline future research directions.

Keywords Transient complex · Macromolecular recognition · Binding shifts · Electron transfer

Introduction

Located in the mitochondrial intermembrane space, yeast cytochrome *c* peroxidase (CcP) is a 34.2 kDa heme enzyme, which catalyzes reduction of hydroperoxides using the electrons provided by its physiological partner cytochrome *c* (Cc). The catalytic mechanism of H₂O₂ reduction involves formation of CcP compound I (CpdI), an intermediate oxidized two equivalents above the CcP(Fe³⁺) resting state (RS) and containing an Fe(IV)=O heme oxyferryl and W191 cation radical (Erman and Vitello 2002). Subsequent CpdI reduction in two one-electron steps involves complex formation with ferrous Cc, intermolecular electron transfer (ET), and product dissociation. Discovered more than 70 years ago (Altschul et al. 1940), CcP has been widely investigated, and its complex with Cc has become a paradigm for understanding biological ET (Erman and Vitello 2002; Volkov et al. 2011). Most of the structural and biophysical studies have been performed on Cc(Fe²⁺):CcP–RS and Cc(Fe³⁺):CcP–RS systems, corresponding to the initial association and the final dissociation complexes, respectively. In addition, cyanide-bound CcP (CcP–CN) was used as a CpdI surrogate, mimicking its spin and coordination states. However, the question remains whether these structural mimics are relevant for description of the reactive Cc(Fe²⁺):CpdI species, transiently populated during the enzyme turnover (Volkov et al. 2011). Another open question concerns formation of a weak, salt-sensitive 2:1 Cc:CcP complex—an ET-active intermediate in one of the kinetic models (Stemp and Hoffman 1993; Zhou and Hoffman 1994)—and location of a hypothetical, low-affinity Cc binding site on CcP (Volkov et al. 2011).

Here we investigate the influence of the proteins' redox and spin-states on their interaction in solution and probe

A. N. Volkov (✉) · N. A. J. van Nuland
Jean Jeener NMR Centre, Structural Biology Brussels, Vrije
Universiteit Brussel, Pleinlaan 2, 1050 Brussels, Belgium
e-mail: ovolkov@vub.ac.be

A. N. Volkov · N. A. J. van Nuland
Department of Structural Biology, VIB, Pleinlaan 2,
1050 Brussels, Belgium

the 2:1 Cc:CcP binding by nuclear magnetic resonance (NMR) spectroscopy. Previous NMR studies relied on either hyperfine-shifted heme resonances of Cc(Fe^{3+}) and CcP–CN detected in one-dimensional (1D) ^1H spectra or backbone amide signals of Cc observed in two-dimensional (2D) heteronuclear single-quantum coherence (HSQC) experiments (see Volkov et al. 2011 and references therein). The latter detection scheme—employing uniformly-labelled ^{15}N Cc and unlabeled, natural abundance CcP—allowed mapping out the Cc surface involved in CcP binding in solution (Worrall et al. 2001). Furthermore, recent studies of the complex by paramagnetic relaxation enhancement (PRE) NMR spectroscopy, which quantified intermolecular paramagnetic effects of spin-labelled CcP on ^{15}N Cc nuclei, established that the crystallographic Cc:CcP orientation is the dominant binding form in solution and delineated a transient encounter complex formed on the path of biomolecular association (Volkov et al. 2006, 2010). However, the ^{15}N Cc-observed experiments alone are insufficient for full structural characterization of the Cc:CcP interaction in solution, highlighting the need for complementary CcP-observed experiments. Very recently, these have been made possible by nearly-complete backbone resonance assignments obtained for perdeuterated, uniformly- $[\text{2H}, \text{13C}, \text{15N}]$ labelled, highly soluble CcP–CN constructs (Volkov et al. 2013). In this work, we carried out the CcP-observed heteronuclear NMR experiments to probe the Cc binding and complement the Cc-based analysis of this protein–protein interaction in solution.

Results and discussion

CcP-observed Cc binding

Given the high structural similarity of the N- or C-terminal His-tagged CcP (His₆CcP and CcPHis₆, respectively) and the native, wild-type (wt) protein (Volkov et al. 2013), most of the backbone amide assignments could be transferred to the 2D ^1H – ^{15}N HSQC spectrum of wt CcP–CN. Stepwise addition of natural-abundance Cc to $[\text{2H}, \text{13C}, \text{15N}]$ wt CcP–CN causes incremental, binding-induced chemical shift perturbations ($\Delta\delta$) of CcP resonances (Fig. 1a). For the spectra acquired in 20 mM sodium phosphate (NaP_i) and 100 mM NaCl (pH 6.0) (the high-salt condition), addition of 1 molar equivalent of Cc(Fe^{3+}) leads to large $\Delta\delta$ of several peaks in both ^1H and ^{15}N dimensions. As the 2:1 complex formation is abolished at high ionic strength (*I*) (Erman and Vitello 2002), these shifts arise from Cc binding to the high-affinity site. Depending on the $\Delta\delta$ size, the affected CcP resonances are in fast or intermediate exchange regime on the NMR chemical shift timescale.

Estimated from the largest $\Delta\delta$ observed in this work, the lower limit of the dissociation rate constant $k_{\text{off}} \geq 890 \text{ s}^{-1}$ for the Cc:CcP–CN complex can be compared to the value of $k_{\text{off}} > 1,200 \text{ s}^{-1}$ reported for the Cc:CcP–RS system (Worrall et al. 2001).

Plotted against the residue number, the $\Delta\delta$ profiles for the wt and His₆CcP–CN are nearly identical (Fig. 1b), confirming that the N-terminal His-tag does not perturb the Cc:CcP interaction (Volkov et al. 2013). In contrast, due to a ~ 60 -fold weaker Cc binding (Volkov et al. 2013), the CcPHis₆–CN shows much smaller chemical shift perturbations, yet the $\Delta\delta$ profile remains very similar to that of the wt protein, indicating that the same CcP area is involved in the complex formation (Fig. 1b). In addition,

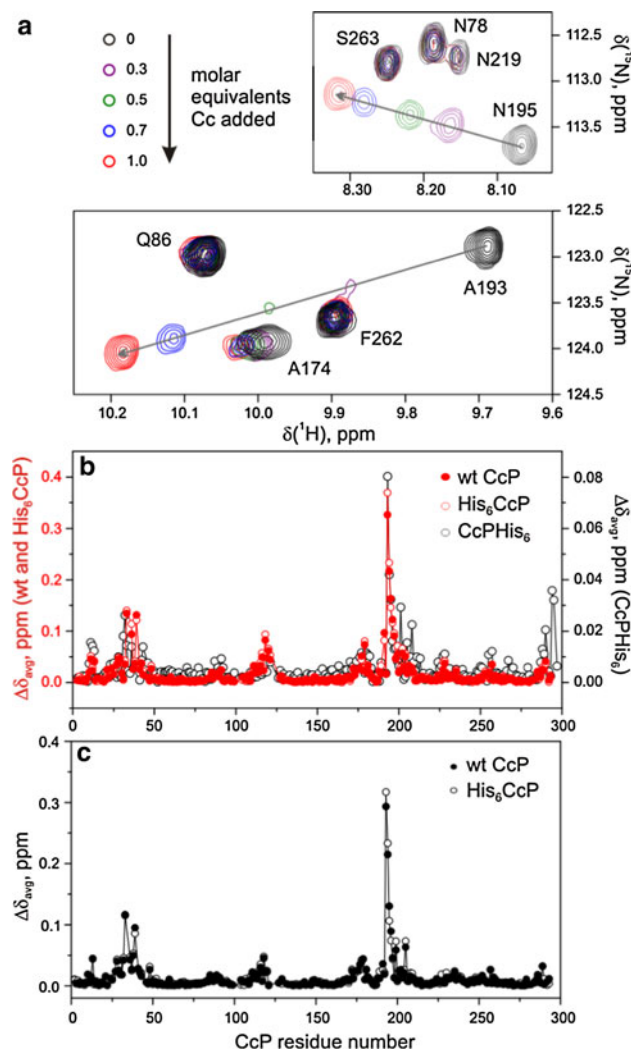


Fig. 1 CcP-observed Cc binding. **a** Chemical shift perturbations of several $[\text{2H}, \text{13C}, \text{15N}]$ wt CcP–CN backbone amide resonances upon binding to Cc(Fe^{3+}). The peak shifts are indicated by the arrows. **b–c** Average amide binding shifts, $\Delta\delta_{\text{avg}}$, of the CcP–CN constructs in the presence of 1 molar equivalent of **b** Cc (Fe^{3+}) or **c** Cc(Fe^{2+}). The experiments were conducted in 20 mM NaP_i and 100 mM NaCl (pH 6.0) at 303 K

large $\Delta\delta$ for the C-terminal part of the protein, including the His-tag residues, indicate that Cc interacts with the C-terminal His-tag, which likely occludes the high-affinity, crystallographic site, leading to weaker binding. The equilibrium shift from the high-affinity binding orientation could result in stronger interaction at the low-affinity site, which makes the CcPHis₆ construct an attractive choice to probe weak Cc:CcP binding in the 2:1 complex (see below). Given the similarity of the $\Delta\delta$ exhibited by the CcP interactions with Cc(Fe³⁺) and Cc(Fe²⁺) (Fig. 1b, c), it appears that the Cc:CcP–CN complex formation is independent of the Cc redox state.

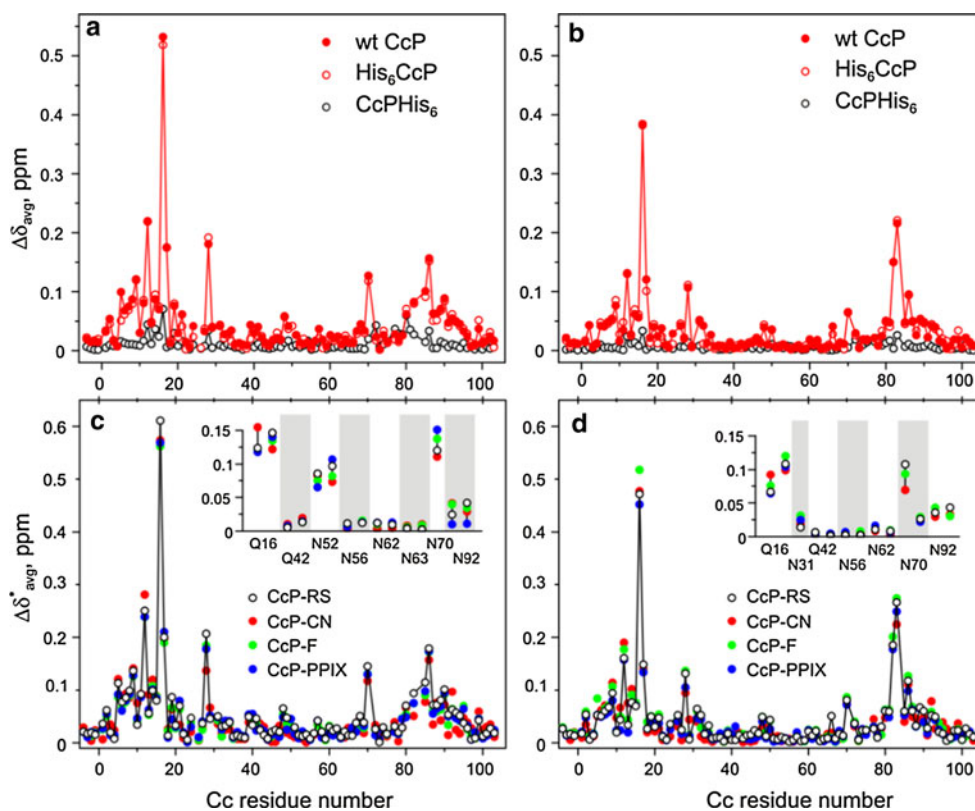
Cc-observed CcP binding

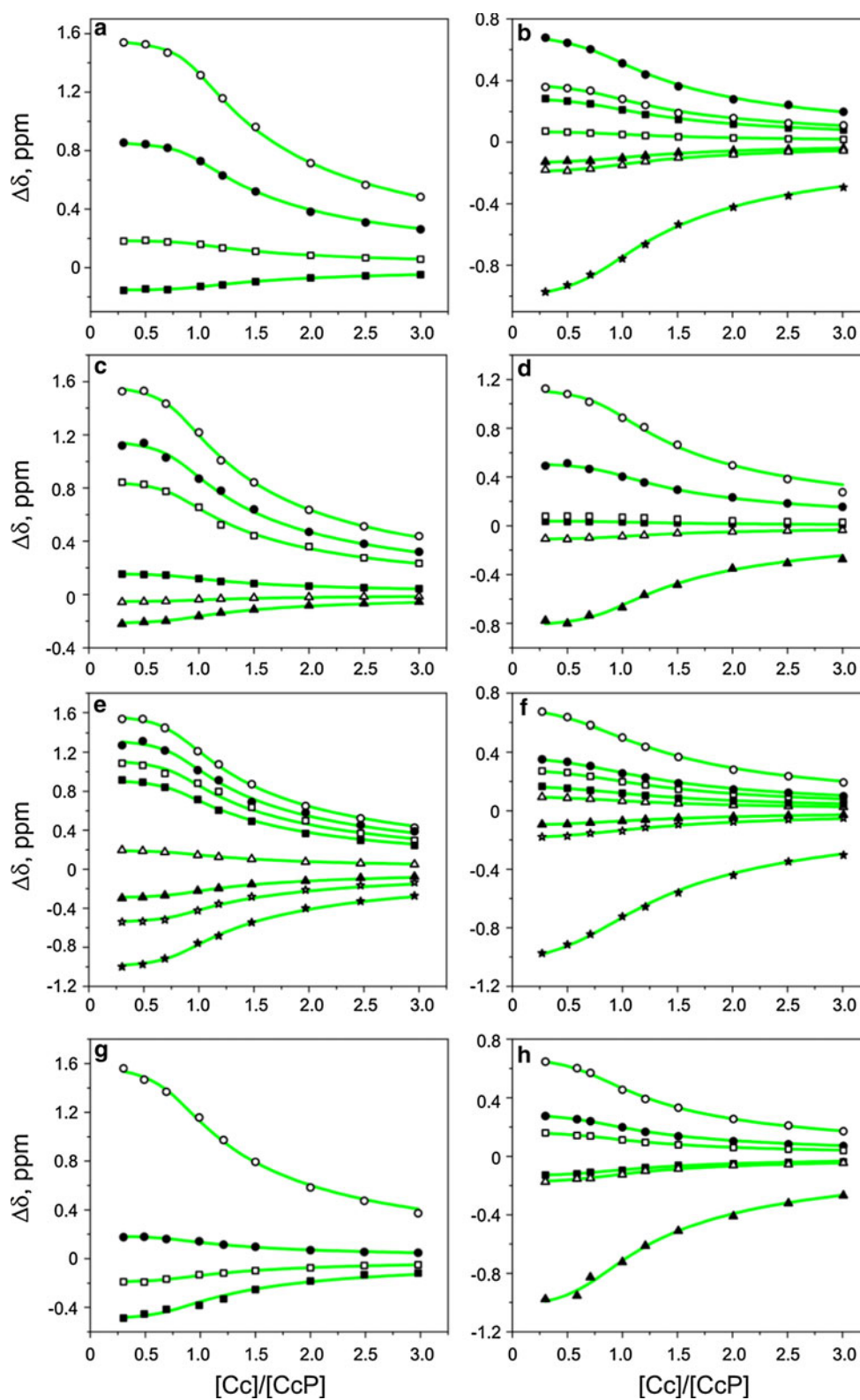
In line with the above findings, the $\Delta\delta$ profiles of Cc-observed wt and His₆CcP binding are virtually identical, while that of CcPHis₆ shows much smaller $\Delta\delta$ (Fig. 2a, b). In this work, we used recently updated resonance assignments of Cc backbone and sidechain amide atoms (Volkov et al. 2012), extending previous Cc-observed $\Delta\delta$ analyses (Volkov et al. 2009; Worrall et al. 2001). Overall, the $\Delta\delta$ plots for the Cc backbone amides are very similar to those reported before for the wt CcP binding, with most of the affected residues located on the front face of the molecule in a patch surrounding the exposed heme edge (Volkov et al. 2009; Worrall et al. 2001). Performed for the first

time, the $\Delta\delta$ analysis of the Cc sidechain amides reveals significant effects for Q16 and N70 groups (Fig. 2c, d, inset). These are consistent with the X-ray structure of the complex, where the latter residue makes the only intermolecular hydrogen bond with the E290 carboxyl of CcP, while the former folds in on itself, forming an H-bond with its own backbone amide (Pelletier and Kraut 1992).

To probe the influence of the CcP spin-state on Cc binding, we performed Cc-observed NMR titrations of CcP–RS (predominantly high-spin, $S = 5/2$ at the present experimental conditions; Yonetani and Anni 1987), fluoride-bound CcP (CcP–F, high-spin, $S = 5/2$), CcP–CN (low spin, $S = 1/2$), and a diamagnetic, $S = 0$ protein containing the iron-free heme analogue protoporphyrin IX (CcP–PPIX). Except for CcP–F, which shows weaker Cc(Fe²⁺) binding, K_D values extracted from the Cc:CcP titration curves (Fig. 3) are very similar (Table 1) and consistent with those found in literature (Erman and Vitello 2002; Volkov et al. 2011). In all complexes studied, Cc(Fe³⁺) binds somewhat more tightly than Cc(Fe²⁺) and, with exception of the Cc(Fe²⁺):CcP–F system, the Cc interaction with CcP–PPIX is a little weaker compared to that with the other CcP forms (Table 1). When extrapolated to the fully bound protein, the $\Delta\delta$ profiles for different complexes are essentially the same (Fig. 2c, d). For all CcP forms studied here, the $\Delta\delta$ values for the interaction with Cc(Fe³⁺) are somewhat larger than those of the

Fig. 2 Cc-observed CcP binding. **a–b** Average amide binding shifts, $\Delta\delta_{\text{avg}}$, of **a** Cc(Fe³⁺) or **b** Cc(Fe²⁺) in the presence of 1 molar equivalent of different CcP constructs. **c–d** $\Delta\delta_{\text{avg}}$ extrapolated to the 100 % bound form ($\Delta\delta_{\text{avg}}^*$) of **c** Cc(Fe³⁺) or **d** Cc(Fe²⁺) in the complex with the different ligation forms of wt CcP. The insets show $\Delta\delta_{\text{avg}}^*$ for the side-chain amides of the indicated Cc residues. The experiments were performed in 20 mM NaP_i and 100 mM NaCl (pH 6.0) at 303 K





corresponding $Cc(Fe^{2+}):CcP$ complexes (Fig. 2c, d). Reported previously for the $Cc:CcP$ -RS system, this phenomenon could arise from the redox-dependent shift in the equilibrium between the stereospecific and encounter

orientations of the protein complex or stem from slight changes in structure and dynamics experienced by Cc in its two redox states (Worrall et al. 2001). Taken together, the present NMR analysis suggests that the $Cc:CcP$ interaction

Fig. 3 NMR chemical shift titrations of different wt CcP forms with ^{15}N Cc. **a** CcP-RS:Cc(Fe^{3+}), **b** CcP-RS:Cc(Fe^{2+}), **c** CcP-CN:Cc(Fe^{3+}), **d** CcP-CN:Cc(Fe^{2+}), **e** CcP-F:Cc(Fe^{3+}), **f** CcP-F:Cc(Fe^{2+}), **g** CcP-PPIX:Cc(Fe^{3+}), and **h** CcP-PPIX:Cc(Fe^{2+}) complexes. Different symbols refer to the chemical shift perturbations ($\Delta\delta$) of the following Cc resonances: **a** heme 3- CH_3 (open circles), Q16 HN (filled circles), Q16 He2b (open squares), and Q16 He2a (filled squares); **b** Q16 HN (filled circles), G83 HN (open circles), F82 HN (filled squares), N70 HN (open squares), T12 HN (filled triangles), V28 HN (open triangles), and T12 N (filled stars); **c** heme 3- CH_3 (open circles), C17 N (filled circles), Q16 HN (open squares), Q16 He2b (filled squares), L9 HN (open triangles), and V28 HN (filled triangles); **d** Q16 N (open circles), N70 N (filled circles), N70 Hd2a (open squares), N70 HN (filled squares), R13 HN (open triangles), and L9 N (filled triangles); **e** heme 3- CH_3 (open circles), Q16 N (filled circles), C17 N (open squares), N70 N (filled squares), Q16 He2b (open triangles), V28 HN (filled triangles), A7 N (open stars), and L9 N (filled stars); **f** Q16 HN (open circles), G83 HN (filled circles), F82 HN (open squares), Q16 He2b (filled squares), K89 HN (open triangles), Q16 He2a (filled triangles), V28 HN (open stars), and T12 N (filled stars); **g** heme 3- CH_3 (open circles), Q16 He2b (filled circles), T12 HN (open squares), and Q16 Ne2 (filled squares); **h** Q16 HN (open circles), F82 HN (filled circles), Q16 He2b (open squares), and T12 HN (filled squares), V28 HN (open triangles), and T12 N (filled triangles). The curves in each panel were fitted simultaneously to a binding model with the shared K_D (Eq. 2). The solid lines show the best fit, with the corresponding K_D values listed in the Table 1. Experiments were performed in 20 mM NaPi and 100 mM NaCl (pH 6.0) at 303 K

is independent of the CcP spin-state and is only weakly affected by the Cc redox status.

Paramagnetic properties of the Cc:CcP complexes

Ferric heme iron atoms of Cc and CcP give rise to paramagnetic effects such as relaxation enhancement and paramagnetic shifts, which can be detected by NMR spectroscopy (Ubbink et al. 2002). For the residues not in direct contact with the heme group, the latter arise from dipolar pseudocontact shifts (PCSs) determined by the magnetic anisotropy of the metal center and the positions of the observed nuclei in the molecular reference frame (Eq. 3 in the Experimental Section). In the absence of redox-dependent conformational changes, PCSs are given by the differences between the chemical shifts of the paramagnetic and diamagnetic protein forms.

Table 1 Equilibrium dissociation constants (K_D s in μM) for the Cc:CcP complexes in 20 mM NaPi and 100 mM NaCl (pH 6.0) at 303 K

CcP form	Cc(Fe^{3+})	Cc(Fe^{2+})
RS	5.5 ± 0.5	10.8 ± 1.0
CN	7.8 ± 1.3	10.5 ± 2.4
F	7.7 ± 1.2	33.5 ± 2.4
PPIX	11.2 ± 2.5	18.7 ± 2.8

Starting from PCSs of the free and CcP-bound Cc obtained in this work, we determined the magnitudes and orientations of the magnetic susceptibility, $\Delta\chi$ tensors in different binding forms (Table 2). With the values being the same within the experimental error, it appears that in all complexes studied, CcP binding does not perturb the $\Delta\chi$ tensor of Cc, in agreement with previous work (Worrall et al. 2001). As illustrated by the crystal structure of the complex (Pelletier and Kraut 1992), the CcP heme group sits far from the Cc:CcP interface. (The closest distance between the CcP heme iron and any of the Cc backbone amides is 21.2 Å for the residue G83.) Consequently, no CcP-derived intermolecular paramagnetic effects on the NMR resonances of the bound Cc were observed. In contrast, due to a close proximity of the Cc heme to the CcP atoms, we could detect small Cc-induced effects (IPCSI < 0.1 ppm) on the backbone amides of CcP-CN. As the Cc:CcP complex is in equilibrium between the transient encounter state and the dominant, crystallographic orientation (Volkov et al. 2006), quantitative interpretation of these PCSs requires the knowledge of the population in the dominant Cc:CcP-CN form, which is a subject of our ongoing investigation.

Cc-CcP interface mapping

Mapping the $\Delta\delta$ of both proteins onto the Cc:CcP X-ray structure reveals that the binding effects are highly localized, with most of the affected residues sitting in the crystallographic interface (Fig. 4). The largest effects are observed for the CcP residues A193–N196 and the Cc groups T12, Q16, C17, and V28. Together with the large effects for the Cc Q16 and N70 sidechains (see above), this interaction pattern is consistent with the X-ray structure, where A193 and A194 of CcP are in close contact with Q16, C17, and the heme group of Cc (Pelletier and Kraut 1992). Thus, the present analysis confirms our earlier

Table 2 Magnetic susceptibility tensors of the free and CcP-bound Cc

System	$\Delta\chi_{ax}$	$\Delta\chi_{rh}$	β	κ	σ^2
Free Cc	3.19 ± 0.05	1.25 ± 0.08	11 ± 1	9 ± 5	0.015
Cc:CcP-RS	3.24 ± 0.06	1.12 ± 0.09	13 ± 1	8 ± 4	0.014
Cc:CcP-CN	3.25 ± 0.06	1.14 ± 0.08	13 ± 1	7 ± 4	0.013
Cc:CcP-F	3.25 ± 0.06	1.07 ± 0.09	13 ± 1	7 ± 4	0.014
Cc:CcP-PPIX	3.27 ± 0.06	1.05 ± 0.09	13 ± 1	7 ± 4	0.014

$\Delta\chi_{ax}$ and $\Delta\chi_{rh}$ are the axial and rhombic components of the $\Delta\chi$ tensor in units of 10^{-32} m³; β and κ are the angles (in degrees) relating the $\Delta\chi$ -tensor frame to the heme-centred molecular coordinate system (Volkov et al. 2012); σ^2 is the statistical variance. Errors are calculated as explained in the Experimental Section

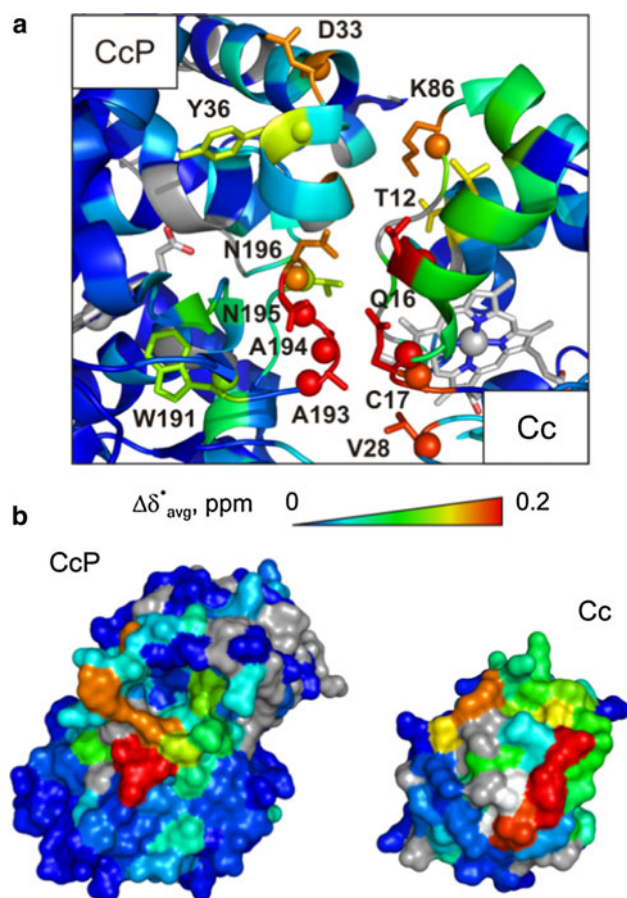


Fig. 4 $\Delta\delta$ mapping of the Cc:CcP binding interface. **a** The contact surface as seen in the X-ray structure of the complex [Protein Data Bank (PDB) entry 2PCC (Pelletier and Kraut 1992)], with the residues colored by $\Delta\delta_{\text{avg}}^*$ for the wt CcP–CN and Cc(Fe³⁺) as defined in the ramp. Residues with $\Delta\delta_{\text{avg}} > 0.1$ ppm are in sticks with the N atoms shown as spheres. Prolines and groups with unassigned/unobserved backbone amide resonances are in grey. The heme groups are shown in sticks, with the iron atoms as grey spheres. Labels identify several groups experiencing large binding effects. **b** The Cc:CcP complex in an open-book view, with the individual proteins rotated by 90° around the vertical axis of the image in **a**. The protein surfaces are coloured as in **a**, with the Cc heme group shown in white

finding that the crystallographic Cc:CcP orientation is preserved in solution (Volkov et al. 2006). Furthermore, given that the Cc:CcP interaction is virtually unaffected by the partners' spin- and redox-states and considering that CcP–CN has the same spin- and heme coordination status as the reactive CpdI species, it appears that the Cc:CcP–CN complex is a good mimic of the catalytically-active Cc:CpdI intermediate.

Probing the weak 2:1 Cc–CcP complex

To search for the elusive, low-affinity binding site, we monitored the Cc interaction with [²H,¹³C,¹⁵N] CcPHis₆–CN, an appealing construct for study of the 2:1 complex

(see above). Compared to the high-salt dataset, the $\Delta\delta$ values in the presence of 1 molar equivalent Cc at low salt are systematically larger (cf. Figs. 1b, 5b). This behaviour reflects a 16-fold increase in the binding affinity at low *I* [$K_D = 18.7 \mu\text{M}$ in 20 mM sodium phosphate (Fig. 5a) as compared to $K_D = 294 \mu\text{M}$ in the presence of 100 mM NaCl (Volkov et al. 2013)]. The low-salt $\Delta\delta$ profile is highly similar to that at the high salt, suggesting that the Cc:CcP structure is not perturbed by changes in ionic strength. Just as at high *I*, the low-salt interaction is independent of the Cc redox state (Fig. 5b, c). Comparison of the data at 1 and 3 molar equivalents of Cc reveals only a small, uniform increase in $\Delta\delta$ due to a higher fraction of the bound protein, with the two $\Delta\delta$ profiles being virtually identical (Fig. 5b). Consistent with the low-salt titration curves (Fig. 5a), no formation of a 2:1 complex is observed. Several causes (or a combination thereof) can account for the absence of binding effects at the low-affinity site. First, the K_D of ≥ 1 mM reported for the second Cc binding event at *I* = 50 mM (pH 6.0) and 298 K (Mauk et al. 1994) could be much higher than this lower limit estimate, giving rise to a small fraction of Cc bound in the 2:1 complex and, hence, minute $\Delta\delta$ not resolved in the present experiments. Second, in the absence of extensive desolvation and close contacts across the interface, which is plausible for this weak interaction mainly driven by complementary electrostatics, the $\Delta\delta$ s are expected to be small and could lie within the experimental error. Finally, extensive averaging of the $\Delta\delta$ over multiple binding orientations caused by protein dynamics could give rise to vanishingly small overall effects (Xu et al. 2008). Currently, we are pursuing a more in-depth analysis to address these issues and probe deeper into the nature of the low-affinity binding site.

Experimental section

Protein samples

Both natural-abundance and uniformly-labelled [²H,¹³C,¹⁵N] CcP and ¹⁵N Cc were prepared as described previously (Volkov et al. 2012, 2013). The CcP–CN and CcP–F were obtained by the addition of a slight excess (typically 1.1–1.2 molar equivalents) of 100 mM NaCN or NaF to the CcP–RS solution. The CcP–PPIX was obtained by the reconstitution of the apo protein with the protoporphyrin IX (Sigma), analogously to the hemin insertion (Volkov et al. 2013), except that the PPIX solution was made in 0.1 M NaOH and 15 % dimethyl sulfoxide (Bhaskar and Poulos 2005). The purified Cc was oxidized with an excess of K₃[Fe(CN)₆] and thoroughly exchanged into an NMR buffer. The reduced Cc(Fe²⁺) was prepared

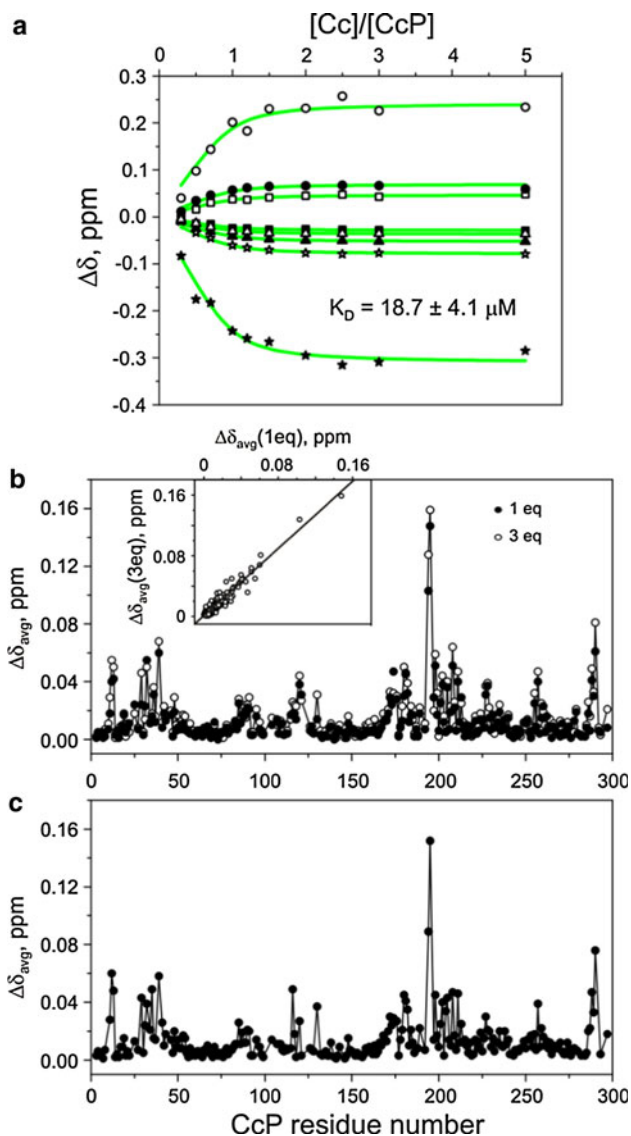


Fig. 5 Cc binding to CcPHis₆ at low ionic strength. **a** The low-salt NMR chemical shift titration of [²H,¹³C,¹⁵N] CcPHis₆-CN with Cc(Fe^{3+}). Chemical shift perturbations ($\Delta\delta$) of the CcP N205 N (open circles), W211 HN (filled circles), Q120 HN (open squares), L46 HN (filled squares), E209 HN (open triangles), L182 HN (filled triangles), N208 HN (open stars), and F202 N (filled stars) resonances, fitted simultaneously to a binding model with the shared K_D (Eq. 1). The solid lines show the best fit, with the K_D value indicated in the plot. The error represents the fitting uncertainty. **b** Average amide binding shifts, $\Delta\delta_{\text{avg}}$, of CcPHis₆-CN in the presence of 1 (filled symbols) and 3 (open symbols) molar equivalents of Cc(Fe^{3+}). The inset shows the correlation plot of $\Delta\delta_{\text{avg}}$ for 1 and 3 Cc(Fe^{3+}) equivalents, with the solid line being the best linear fit of the data (slope = 1.11, $r^2 = 0.934$). **c** Average amide binding shifts, $\Delta\delta_{\text{avg}}$, of CcPHis₆-CN in the presence of 3 molar equivalents of Cc(Fe^{2+}). All experiments were performed in 20 mM NaP_i (pH 6.0) at 298 K

by the addition of a twofold molar excess of sodium ascorbate to the Cc(Fe^{3+}) solution. The protein concentrations were calculated from the UV-vis spectra using the extinction coefficients $\epsilon_{408} = 98.0$ (CcP-RS) (Yonetani

and Anni 1987), $\epsilon_{423} = 97.3$ (CcP-CN) (Volkov et al. 2013), $\epsilon_{407} = 127.2$ (CcP-F) (Volkov et al. 2013), $\epsilon_{408} = 96.0$ (CcP-PPIX) (Bhaskar and Poulos 2005), and $\epsilon_{410} = 106.1$ (oxidized Cc) (Margoliash and Frohwirt 1959) $\text{mM}^{-1}\text{cm}^{-1}$. NMR samples were prepared in 20 mM NaP_i (pH 6.0) (low-salt condition) or 20 mM NaP_i and 100 mM NaCl (pH 6.0) (high-salt condition) and contained 6 % ²H₂O for the lock.

NMR spectroscopy

The 1D ¹H and 2D ¹H-¹⁵N HSQC experiments were conducted on Varian NMR Direct-Drive System 600 and 800 MHz spectrometers, the latter equipped with a salt tolerance triple-resonance PFG-Z cold probe. For the [²H,¹³C,¹⁵N] CcP samples, TROSY-selected HSQC experiments were used. All NMR data were processed in NMRPipe (Delaglio et al. 1995) and analyzed in CCPN (Vranken et al. 2005). For all observed backbone amide resonances, chemical shift assignments of the [²H,¹³C,¹⁵N] His₆CcP-CN reported in our earlier work (Volkov et al. 2013) could be transferred to the HSQC spectrum of the [²H,¹³C,¹⁵N] wt CcP-CN, once again attesting to the high structural similarity of the wt and His-tagged proteins. Chemical shift assignment for the Cc in both oxidation states were taken from literature (Volkov et al. 2012).

NMR titrations

The Cc-observed, reverse titrations (Fig. 3) were performed in the high-salt condition at 303 K by incremental addition of a concentrated ¹⁵N Cc stock solution to the CcP samples at the initial concentration of 0.3 mM. The CcPHis₆-detected, direct titration at low salt and 298 K (Fig. 5a) was carried out in a similar fashion, by stepwise addition of a 3.3 mM Cc(Fe^{3+}) solution to a 0.3 mM [²H,¹³C,¹⁵N] CcPHis₆-CN sample. At each increment, changes in chemical shifts of the protein resonances were monitored in ¹H-¹⁵N HSQC spectra. The direct and reverse titration curves were analyzed with a two-parameter non-linear least squares fit using a one-site binding model corrected for the dilution effect (Kannt et al. 1996) as given in Equations 1 and 2, respectively.

$$\Delta\delta_{\text{binding}} = 0.5\Delta\delta_0 \left(A - \sqrt{A^2 - 4R} \right) \tag{1}$$

$$A = 1 + R + K_D \frac{[Cc]_0 + R[CcP]_0}{[Cc]_0[CcP]_0},$$

$$\Delta\delta_{\text{binding}} = 0.5\Delta\delta_0 \left(A - \sqrt{A^2 - 4/R} \right) \tag{2}$$

$$A = 1 + 1/R + K_D \frac{[Cc]_0 + R[CcP]_0}{R[Cc]_0[CcP]_0},$$

where $\Delta\delta_{\text{binding}}$ is the chemical shift perturbation at a given protein ratio; $\Delta\delta_0$ is the chemical shift perturbation at 100 % Cc bound; R is the [Cc]/[CcP] ratio at a given point; [CcP]₀ and [Cc]₀ are the concentrations of the starting sample and the titrant stock solution, respectively; and K_D is the equilibrium dissociation constant. Thus, $\Delta\delta_{\text{binding}}$ and R are the dependent and independent variables, respectively, and $\Delta\delta_0$ and K_D are the fitted parameters.

Chemical shift perturbation analysis

The samples contained 0.3–0.4 mM of the free ¹⁵N Cc or [²H, ¹³C, ¹⁵N] CcP–CN constructs and their complexes with the corresponding natural-abundance binding partner. The average amide chemical shift perturbations ($\Delta\delta_{\text{avg}}$) were calculated as $\Delta\delta_{\text{avg}} = (\Delta\delta_{\text{N}}^2/50 + \Delta\delta_{\text{H}}^2/2)^{0.5}$, where $\Delta\delta_{\text{N}}$ and $\Delta\delta_{\text{H}}$ are the chemical shift perturbations of the amide nitrogen and proton, respectively. To obtain $\Delta\delta_{\text{avg}}$ extrapolated to the 100 % bound form ($\Delta\delta_{\text{avg}}^*$), the $\Delta\delta_{\text{avg}}$ values were divided by the fraction of the protein bound, calculated from the affinity constants obtained in this work.

Paramagnetic NMR analysis

The PCS is given by Equation 3 (Ubbink et al. 2002):

$$\text{PCS} = \frac{1}{12\pi} r^{-3} [\Delta\chi_{ax} (3 \cos^2 \theta - 1) + 3/2 \Delta\chi_{rh} \sin^2 \theta \cos 2\phi] \quad (3)$$

where r , θ , and ϕ are the polar coordinates of the nuclear spin with respect to the principal axes of the magnetic susceptibility tensor ($\Delta\chi$), and $\Delta\chi_{ax}$ and $\Delta\chi_{rh}$ are, respectively, the axial and rhombic components of the $\Delta\chi$ tensor.

The $\Delta\chi$ tensors were calculated from experimental PCSs of Cc HN atoms and the Cc X-ray structure [PDB ID 1YCC (Louie and Brayer 1990)] with Numbat (Schmitz et al. 2008). The residues that exhibit redox-dependent conformational changes (Volkov et al. 2012) or are in direct contact with the heme group (and, thus, experience non-negligible contact shifts) were excluded from the analysis. The calculated tensors were corrected for the residual anisotropic chemical shifts (John et al. 2005) using the correction term implemented in Numbat (Schmitz et al. 2008). The errors on the $\Delta\chi$ parameters were estimated with a Monte-Carlo protocol (Schmitz et al. 2008) by adding 10 % of Gaussian noise to the atomic coordinates and experimental PCS values and randomly excluding 10 % of the working PCS dataset. The agreement between the observed and calculated PCSs was assessed from a statistical variance (σ^2), given by $\sigma^2 = [\sum(\text{PCS}_{\text{obs}} - \text{PCS}_{\text{cal}})^2]/(n-5)$, with the summation carried over all atoms used in the fitting (n).

Acknowledgments We thank Karen Van de Water for help with analysis of the low-salt data and Yann Sterckx and Sophie Vanwetwinkiel for the critical reading of the manuscript. A. N. V. is an FWO Post-Doctoral Researcher. We acknowledge the financial support from VIB and the Hercules Foundation.

References

- Altschul AM, Abrams R, Hogness TR (1940) Cytochrome *c* peroxidase. *J Biol Chem* 136:777–794
- Bhaskar B, Poulos TL (2005) The 1.13-Å structure of iron-free cytochrome *c* peroxidase. *J Biol Inorg Chem* 10:425–430
- Delaglio F, Grzesiek S, Vuister GW, Zhu G, Pfeifer J, Bax A (1995) NMRPipe: a multidimensional spectral processing system based on UNIX pipes. *J Biomol NMR* 6:277–293
- Erman JE, Vitello LB (2002) Yeast cytochrome *c* peroxidase: mechanistic studies via protein engineering. *Biochim Biophys Acta* 1597:193–220
- John M, Park AY, Pintacuda G, Dixon NE, Otting G (2005) Weak alignment of paramagnetic proteins warrants correction for residual CSA effects in measurements of pseudocontact shifts. *J Am Chem Soc* 127:17190–17191
- Kannt A, Young S, Bendall DS (1996) The role of acidic residues of plastocyanin in its interaction with cytochrome *f*. *Biochim Biophys Acta* 1277:115–126
- Louie GV, Brayer GD (1990) High-resolution refinement of yeast *iso*-1-cytochrome *c* and comparisons with other eukaryotic cytochromes *c*. *J Mol Biol* 214:527–555
- Margoliash E, Frohwirt N (1959) Spectrum of horse-heart cytochrome *c*. *Biochem J* 71:570–572
- Mauk MR, Ferrer JC, Mauk AG (1994) Proton linkage in formation of the cytochrome *c*–cytochrome *c* peroxidase complex: electrostatic properties of the high- and low-affinity cytochrome binding sites on the peroxidase. *Biochemistry* 33:12609–12614
- Pelletier H, Kraut J (1992) Crystal structure of a complex between electron transfer partners, cytochrome *c* peroxidase and cytochrome *c*. *Science* 258:1748–1755
- Schmitz C, Stanton-Cook MJ, Su X-C, Otting G, Huber T (2008) Numbat: an interactive software tool for fitting $\Delta\chi$ -tensors to molecular coordinates using pseudocontact shifts. *J Biomol NMR* 41:179–189
- Stemp EDA, Hoffman BM (1993) Cytochrome *c* peroxidase binds two molecules of cytochrome *c*: evidence for a low-affinity, electron-transfer-active site on cytochrome *c* peroxidase. *Biochemistry* 32:10848–10865
- Ubbink M, Worrall JAR, Canters GW, Groenen EJJ, Huber M (2002) Paramagnetic resonance of biological metal centers. *Annu Rev Biophys Biomol Struct* 31:393–422
- Volkov AN, Worrall JAR, Holtzmann E, Ubbink M (2006) Solution structure and dynamics of the complex between cytochrome *c* and cytochrome *c* peroxidase determined by paramagnetic NMR. *Proc Natl Acad Sci USA* 103:18945–18950
- Volkov AN, Bashir Q, Worrall JAR, Ubbink M (2009) Binding hot spot in the weak protein complex of physiological redox partners yeast cytochrome *c* and cytochrome *c* peroxidase. *J Mol Biol* 385:1003–1013
- Volkov AN, Ubbink M, van Nuland NAJ (2010) Mapping the encounter state of a transient protein complex by PRE NMR spectroscopy. *J Biomol NMR* 48:225–236
- Volkov AN, Nicholls P, Worrall JAR (2011) The complex of cytochrome *c* and cytochrome *c* peroxidase: the end of the road? *Biochim Biophys Acta* 1807:1482–1503
- Volkov AN, Vanwetwinkiel S, Van de Water K, van Nuland NAJ (2012) Redox-dependent conformational changes in eukaryotic

- cytochromes revealed by paramagnetic NMR spectroscopy. *J Biomol NMR* 52:245–256
- Volkov AN, Wohlkonig A, Soror SH, van Nuland NAJ (2013) Expression, purification, characterization, and solution nuclear magnetic resonance study of highly-deuterated yeast cytochrome *c* peroxidase with enhanced solubility. *Biochemistry* 52:2165–2175
- Vranken WF, Boucher W, Stevens TJ, Fogh RH, Pajon A, Llinas M, Ulrich EL, Markley JL, Ionides J, Laue ED (2005) The CCPN data model for NMR spectroscopy: development of a software pipeline. *Proteins* 59:687–696
- Worrall JAR, Kolczak U, Canters GW, Ubbink M (2001) Interaction of yeast *iso-1*-cytochrome *c* with cytochrome *c* peroxidase investigated by [^{15}N , ^1H] heteronuclear NMR spectroscopy. *Biochemistry* 40:7069–7076
- Xu X, Reinle W, Hannemann F, Konarev PV, Svergun DI, Bernhardt R, Ubbink M (2008) Dynamics in a pure encounter complex of two proteins studied by solution scattering and paramagnetic NMR spectroscopy. *J Am Chem Soc* 130:6395–6403
- Yonetani T, Anni H (1987) Yeast cytochrome *c* peroxidase. Coordination and spin states of heme prosthetic group. *J Biol Chem* 262:9547–9554
- Zhou JS, Hoffman BM (1994) Stern-Volmer in reverse: 2:1 stoichiometry of the cytochrome *c*-cytochrome *c* peroxidase electron-transfer complex. *Science* 265:1693–1696